

A 3D printed pure copper drift tube linac prototype


Cite as: Rev. Sci. Instrum. **93**, 023304 (2022); <https://doi.org/10.1063/5.0068494>

Submitted: 25 August 2021 • Accepted: 01 February 2022 • Published Online: 22 February 2022

 M. Mayerhofer, J. Mitteneder and G. Dollinger

COLLECTIONS

 This paper was selected as Featured

 This paper was selected as Scilight



View Online



Export Citation



CrossMark

ARTICLES YOU MAY BE INTERESTED IN

[A large octupole magnetic trap for research with atomic hydrogen](#)

Review of Scientific Instruments **93**, 023201 (2022); <https://doi.org/10.1063/5.0070037>

[A study of space charge induced non-linearity in the Single Line Of Sight camera](#)

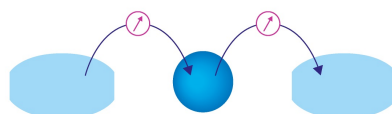
Review of Scientific Instruments **93**, 023505 (2022); <https://doi.org/10.1063/5.0071957>

[X-ray diagnostics of ECR ion sources—Techniques, results, and challenges](#)

Review of Scientific Instruments **93**, 021102 (2022); <https://doi.org/10.1063/5.0076321>

Webinar

Interfaces: how they make
or break a nanodevice



March 29th – Register now



Zurich
Instruments

A 3D printed pure copper drift tube linac prototype



Cite as: Rev. Sci. Instrum. 93, 023304 (2022); doi: 10.1063/5.0068494

Submitted: 25 August 2021 • Accepted: 1 February 2022 •

Published Online: 22 February 2022



View Online



Export Citation



CrossMark

M. Mayerhofer,^{a)}  J. Mitteneder, and G. Dollinger

AFFILIATIONS

Institute for Applied Physics and Measurement Technology, Bundeswehr University Munich, 85577 Neubiberg, Bavaria, Germany

^{a)} Author to whom correspondence should be addressed: michael.mayerhofer@unibw.de

ABSTRACT

Radio frequency cavities are among the most challenging and costly components of an accelerator facility. They are usually manufactured in individual parts, which are then joined by complex processes, e.g., several brazing steps. 3D printing has become an alternative to these conventional manufacturing methods due to higher cost efficiency, freedom in design, and recent achievement of high print quality for pure copper. A fully functional 3 GHz drift tube linac (DTL) prototype was 3D printed in one piece, made from pure copper by selective laser melting (SLM). To achieve a higher surface quality, the DTL geometry was optimized for the SLM process. The DTL design is related to the design of the DTL part of the side-coupled DTL modules used in linac-based proton therapy facilities. The quality factor (8750) and the shunt impedance per unit length ($102 \frac{\text{m}\Omega}{\text{m}}$) of the printed prototype are already comparable to traditionally manufactured DTL structures and can be further enhanced by surface treatments.

© 2022 Author(s). All article content, except where otherwise noted, is licensed under a Creative Commons Attribution (CC BY) license (<http://creativecommons.org/licenses/by/4.0/>). <https://doi.org/10.1063/5.0068494>

I. INTRODUCTION

More than 30 000 electron and ion accelerator facilities are operated worldwide for a wide variety of applications.¹ Well-known examples include linear accelerators, cyclotrons, and synchrotrons for fundamental physics research or for applications such as radiotherapy for the treatment of tumors.^{2–5} The basic components for many of these facilities are radio frequency (RF) structures. They are used as RF cavities for accelerating particles as passive components, e.g., for transmitting RF power (waveguides), and in RF power amplifiers (klystron amplifiers). Their production is usually quite complicated. For example, normal conducting cavities with complex internal geometries, such as drift tubes and cooling channels, cannot be manufactured in a single step. For this reason, individual parts are manufactured, which are subsequently joined by brazing or other processes in order to realize, for example, the lowest possible surface resistance and, if necessary, vacuum tightness or complex cooling channels.^{6–8} The manufacturing process of RF structures often requires many of these subsequently executed precision soldering/brazing steps. This limits the freedom in design and is a major source of potential defects. Combined with the fact that

RF structures are often prototypes, one-offs, or small batches, the manufacturing process of these structures accounts for a large part of the main expense in building an accelerator facility.⁹ Therefore, manufacturing processes that allow new degrees of freedom in resonator design and the creation of more efficient or less expensive components are the subject of the current research worldwide.

3D printing or additive manufacturing techniques,¹⁰ which have been continuously improved since 1980, are attracting increasing attention for the manufacturing of RF structures. Compared to traditional manufacturing processes, their unique advantages are the greater freedom in design and time saving. On the other hand, critical points for 3D printing of such structures are the shape accuracy, the surface quality, and limitations in the choice of materials. Thus, only a few years ago, the potential of 3D printing for RF components was considered rather low.¹¹ Nevertheless, research continued on the 3D printing topic and due to the low importance of shape accuracy for broadband devices (e.g., waveguides), prototypes were successfully manufactured and tested in this field.^{11–13} So far, attempts to print cavity resonators have concentrated almost exclusively on superconducting structures as presented in Refs. 14–16, although normal conducting structures are much more common.

The reason for this is that normal conducting cavities are usually made of copper, which is not well suited as a material for 3D printing due to its high thermal conductivity, high melting point, and high reflection to laser light near IR (normally used in laser based machines).¹⁷ Nevertheless, due to the high potential of 3D printing with high-purity copper for almost all industrial sectors due to its excellent electrical and thermal properties, significant effort and progress have been made in recent years. Finally, the electron beam melting (EBM) 3D printing technique was optimized to print high-purity copper with density, electrical conductivity, and thermal conductivity (nearly) equivalent to wrought copper.¹⁸ However, EBM is not yet widespread in the business-to-business or customer segment, which means that researchers have to put a lot of effort into developing a printing process suitable for the desired structure, which is a great challenge and requires cooperation with other institutions. First attempts to print a prototype of a normal conducting klystron output cavity with EBM are currently in progress at the Stanford Linear Accelerator Center (SLAC) and North Carolina State University. To date, however, this research project has only been presented in a newspaper article published by SLAC itself.¹⁹ Two years ago, selective laser melting (SLM) was established as a further 3D printing process to print high-purity copper with high quality.²⁰ The advantages of SLM compared to EBM are a slightly better surface quality and shape accuracy. Besides, commercial platforms allow easy access to SLM technology and promise consistently high quality.²¹ The disadvantage of the SLM process is that overhanging structures above a certain dimension must be printed with additional support structures in order to maintain the print quality and shape accuracy. The printed support structures have to be removed again after the printing process, which is a challenge especially for small cavities or difficult accessible internal geometries. Internal geometries that are difficult to access and which were supported during printing often have reduced surface quality due to the limited post-processing options. Cavities must therefore be designed in such a way that the support structures can be easily removed after printing or support structures can be avoided.

This work shows for the first time a drift tube linear accelerator (linac) prototype [drift tube linac (DTL) prototype] with a cavity printed entirely from pure copper comparable in performance and properties to traditionally fabricated structures currently in use. To show the potential for research and industry, a drift tube linac structure was chosen, which is comparable to the drift tube linac part of the Side Coupled Drift Tube linacs (SCDTLs) used in prototypes for proton radiotherapy linac systems as currently being developed by ENEA^{22,23} (TOP-IMPLART project) or AVO-ADAM S.A.²⁴ (LIGHT project). The DTL prototype is designed with CST Microwave Studio^{®25} to operate at a resonance frequency of ~2998 MHz. The cavity cells are operated in the fundamental TM_{010} -mode, and the standing wave mode is 2π . Furthermore, the printed DTL prototype will be used as a buncher unit in a currently planned preclinical minibeam irradiation facility, which consists basically of a tandem pre-accelerator and a 3 GHz linac post-accelerator.²⁶ The buncher unit optimizes the longitudinal phase space of a 16 MeV proton tandem beam (DC) to the phase space accepted by the post-accelerator and thus increases the particle transmission through the post-accelerator by a factor of 3. The unit cell length of the cavity of the DTL prototype is therefore adapted

to 16 MeV protons. The maximum transmission through the post-accelerator is achieved for an axial voltage (buncher amplitude) of 42 kV. To demonstrate that the printing process can be transferred completely to an industrial supplier, SLM was chosen for production. The main task is to adapt the cavity geometry to the needs of both, optimum performance as an accelerator structure and to overcome the limitations of the SLM process as discussed earlier.

II. MATERIALS AND METHODS

A. Design of the DTL prototype

The cavity design of the DTL prototype and thus the electromagnetic (EM) field distribution in the cavity are elaborated with CST Microwave Studio[®] (CST).²⁵ The specific resonance frequency of ~2998 MHz is achieved in an iterative process by repeatedly modifying the cavity geometry using the CAD program SolidEdge^{®27} and subsequently calculating the resonance frequency using the Eigenmode Solver, which is provided by CST. The initial geometry for this process is roughly based on the DTL structure developed by ENEA and used in the TOP-IMPLART project as part of the second Side Coupled Drift Tube Linac (SCDTL-2) module.^{22,23} The unit cell length of the DTL prototype is adjusted to a proton energy of 16 MeV ($\beta = \frac{v}{c} = 0.182$). This cavity geometry was chosen for the following two reasons:

1. The DTL prototype can thus be used as a 3 GHz buncher unit in a planned preclinical proton minibeam irradiation facility, which basically consists of a tandem Van de Graaff pre-accelerator and a linear post-accelerator.²⁶ The buncher unit increases the transmission through the post-accelerator by a factor of 3 by adjusting the 16 MeV proton tandem beam to the longitudinal accepted phase space of the linac.
2. A 3 GHz buncher unit with a comparable traditionally manufactured cavity has already been realized,²⁸ allowing a comparison between 3D printing and traditional manufacturing. The traditionally manufactured cavity is further referred to as the reference cavity, and its longitudinal section and transversal section are shown in Figs. 1(a) and 1(b), respectively. A section of stem and drift tube is shown in Fig. 1(c). As the DTL prototype, the reference cavity is adapted from the drift tube part of the second Side Coupled Drift Tube Linac (SCDTL-2) structure of the TOP-IMPLART-LINAC.²³ The cavity consists of five DTL unit cells. For use in the preclinical irradiation facility, the cavity geometry of the SCDTL-2 structure (insertion energy 16.5 MeV) was optimized for 16 MeV. Ports are provided for excitation as well as pickup loop and a variable as well as a fixed copper tuner. The exact prescribed resonance frequency of 2.997 92 GHz is obtained at a temperature of 42 °C. To achieve and maintain this temperature, the stems and corpus are traversed by cooling channels. All parts of the reference cavity [stems with drift tubes, corpus parts, and CF flanges] are joined vacuum-tight by brazing. The fully assembled buncher unit (reference DTL cavity) is shown in Fig. 1(d).

Figure 2 shows the developed printable cavity geometry of the DTL prototype and the negative of the cooling channels going through the cavity according to the suggestions in our patent.²⁹

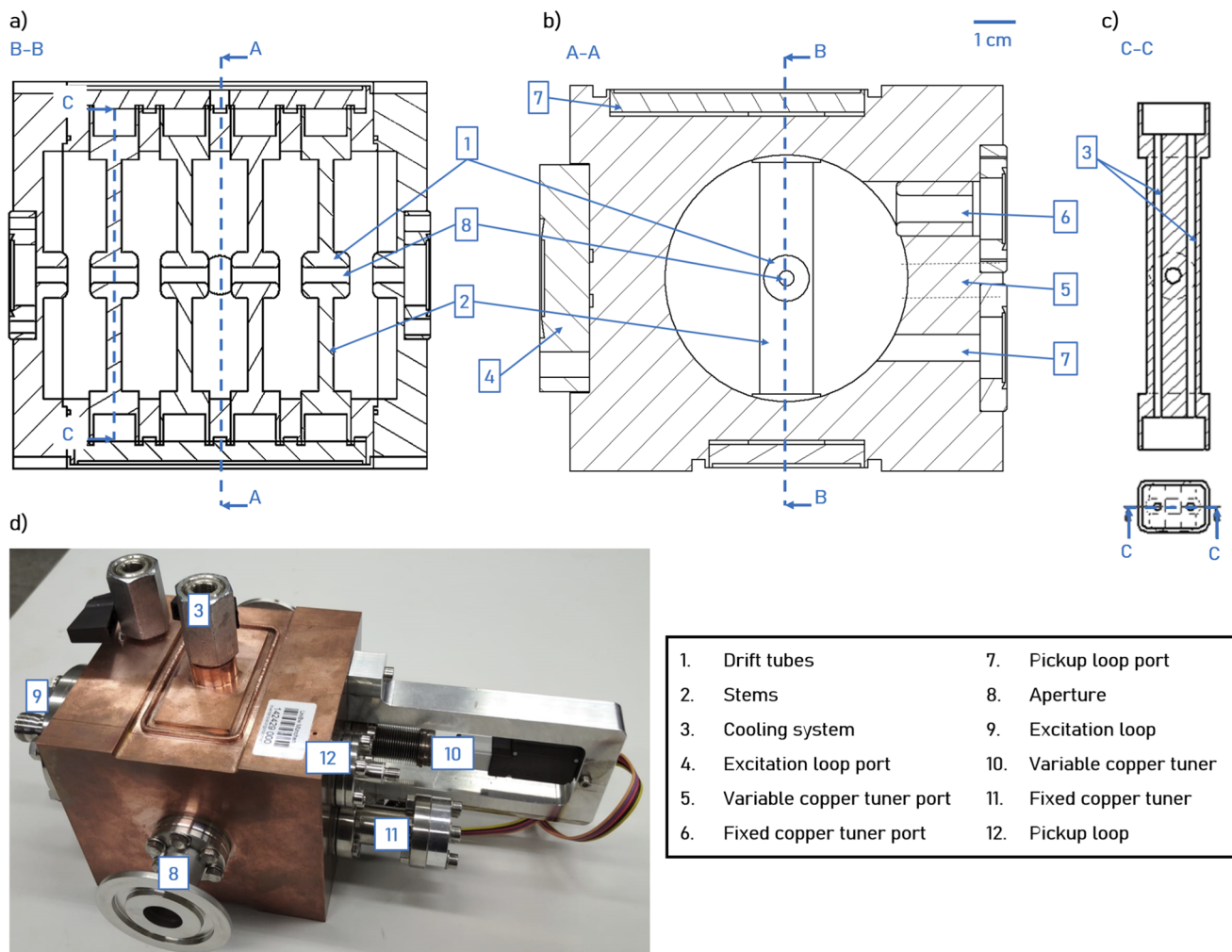


FIG. 1. (a) Longitudinal and (b) transversal sections of the traditionally manufactured reference DTL cavity. (c) Section of stem and drift tube with integrated cooling channels. (d) Fully assembled 3 GHz buncher unit.

The cavity walls and four drift tubes, each supported by only one stem, form five DTL unit cells. The length of a unit cell is 18.2 mm. Accesses are provided for pickup and excitation loop, variable copper tuner, and fixed copper tuner. To increase the frequency stability, linear accelerators are often operated at a constant temperature using a cooling system integrated into the cavity geometry. In our layout, the coolant is directed through individual channels to each stem, flows through one side of each stem to the drift tubes, flows around the drift tubes, and is returned through the other side of the stems. The individual cooling channels of the stems are connected by large supplying channels. The minimum cross section of the cooling system is 32 mm². This is about a factor of 1.5 larger than the cooling system of a comparable DTL structure from the TOP-IMPLART project.⁸ The design with only one stem per drift tube with an integrated cooling system was chosen to illustrate

the potential of 3D printing that increases the freedom of design. Single stem designs are difficult to realize with these cavity dimensions using traditional manufacturing methods. This is mainly due to the difficulty in controlling the brazing process as it was also used for the reference cavity. However, a one-stem geometry promises higher performance due to lower EM-field interference compared to two-stem designs. For example, for the DTL modules of the TOP-IMPLART project, a 15% reduction in shunt impedance was simulated for a geometry with two stems instead of one stem per drift tube.⁸ The developed DTL geometry is self-supporting during the SLM process, which is why there is no need for additional support structures. Thus, a high surface quality can be achieved even without reworking the inner geometry. The geometry modifications that enable the self-supporting printing process are mainly the drop-shaped form of the cavity at the top, the arch structure below

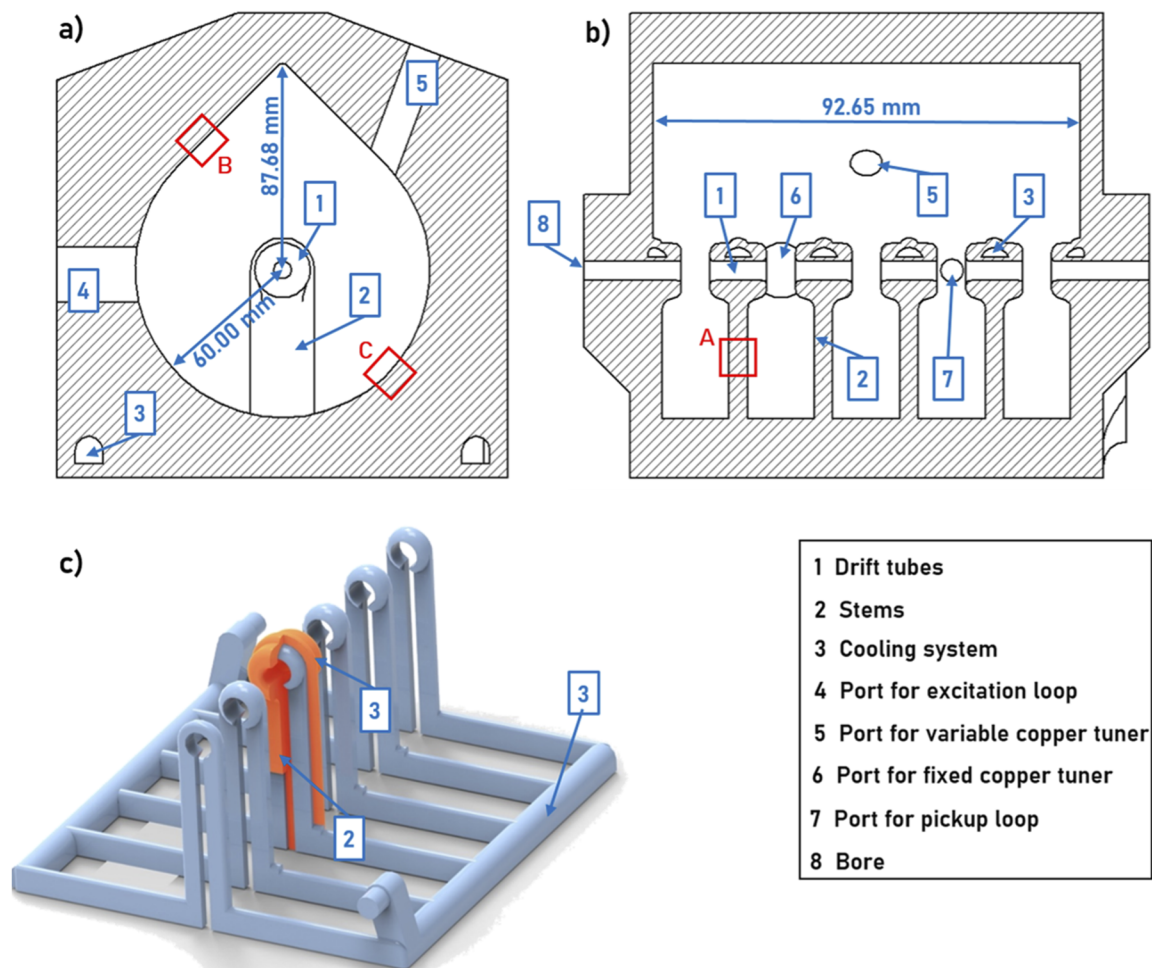


FIG. 2. (a) Front section and (b) longitudinal section of the cavity geometry of the DTL prototype. The red boxes A, B, and C indicate the parts of the geometry where the surface roughness R_a is measured. (c) Negative of the cooling system that passes through the cavity of the DTL prototype (3) with a stem cut open for illustration (2).

the drift tubes, and the arch-shaped ceilings of the cooling channels. The largest overhangs of a traditional DTL structure are, thus, avoided, which greatly increases the print quality. The most important design parameters of the DTL prototype and the reference cavity are summarized in Table I. In order to characterize the geometric modifications required for the printing process, two dimensions are specified for the cavity diameter, which are also displayed in Fig. 2. The shunt impedance of the reference cavity was determined using a Q3D magnetic spectrograph and the 16 MeV proton beam from the tandem Van de Graaff accelerator at the Maier-Leibnitz Laboratory in Garching. The measurement setup, the results, and the calculation of the uncertainty have already been published.²⁸ Within the measurement uncertainties, simulated and measured quality factor and shunt impedance of the reference cavity agree. It can therefore be assumed that the cavity designed for 3D printing would achieve the simulated values (see Table I) if it were manufactured using traditional methods. The geometric accuracy describes the maximum deviation of the geometric dimensions of the reference cavity after

the brazing process compared to the assumed dimensions in the CST simulation. It was not determined on the reference cavity itself, since its dimensions do not allow measurement of the internal geometry after brazing. Instead, it is assumed that the reference cavity achieves the same geometric accuracy as other cavities with the same geometry made by the same manufacturer.²² The surface roughness was determined due to the same geometric limitation on the outer surface of the cavity. The specified value results from the averaging of three individual measurements at different positions on the outer surface. Since the inner and outer surfaces were machined with the same milling tool by the same computer numerical control (CNC) milling machine, it can be assumed that they are identical.

B. Manufacturing of the DTL prototype

The cavity of the DTL prototype was ordered from PROTIQ GmbH²¹ via their online marketplace. It was fabricated from pure copper (minimum copper mass fraction: 99.9%, specific electrical

TABLE I. CST-simulated and measured design parameters of the reference DTL cavity ($f_R \approx 2998$ MHz) as well as the simulated parameters of the 3D printed cavity. The two cavity diameters of the 3D printed cavity are specified in Fig. 2.

	3D printed cavity Simulation	Reference cavity	
		Simulation	Measurement
Quality factor Q_0	13 017	10 600	10 350 \pm 530
Shunt impedance per unit length R_L [$\frac{M\Omega}{m}$]	138	117	106 \pm 13
Cavity diameter D (mm)	60.0/87.9	62.0	
Drift tube diameter d (mm)	12	12	
Aperture radius r (mm)	2	2	
Overall length L (mm)	91.1	91.1	
Gap length a (mm)	6.14	6.24	
Geometrical accuracy a (μm)			≈ 10
Averaged surface roughness R_a (μm)			<1

conductivity: $58 \frac{\text{MS}}{\text{m}}$, thermal conductivity: $400 \frac{\text{W}}{\text{mK}}$, and density: $8.9 \frac{\text{g}}{\text{cm}^3}$) by selective laser melting. The cavity was printed perpendicular to the beam axis (z axis) and parallel to the stems. For mounting the rubber-sealed vacuum CF-flanges for pickup and excitation loop, variable copper tuner, and fixed copper tuner, as well as for the valves of the cooling system (G1/4"), threads were cut. The contact surfaces of the rubber seals with the cavity were milled plane in order to increase the vacuum tightness. For comparison with the traditionally manufactured reference cavity, the average surface roughness R_a of the inner cavity surfaces is to be determined. However, R_a cannot be measured directly on the internal geometry of the DTL prototype without destroying it. Therefore, three samples were cut out of the existing printed test geometries, comparable to the red marked geometry parts A, B, and C of the DTL prototype in Fig. 2. Subsequently, the averaged surface roughness R_a of the individual samples was determined with the aid of a 3D laser confocal scanning microscope (KEYENCE VK-X3000). Since, according to the CST simulation, the highest current density is localized on the stem surface (A), its roughness is of particular interest.

C. RF performance measurement

The performance of the DTL prototype is characterized by the unloaded quality factor Q_0 and the shunt impedance per unit length (L), R_L .^{4,30} Q_0 was determined by measuring the -3 dB bandwidth of the resonance curve. To determine R_L , the E-field distribution along the beam axis of the DTL prototype was evaluated for the fundamental mode (TM_{010}) by pulling a small dielectric object (perturbation body) attached to a thin string through the cavity (bead-pulling measurement).^{31,32} According to the cavity perturbation theory,^{33,34} the change in the resonance frequency is a function of the electric and magnetic field strength at the location of the perturbation body and the characteristics of the perturbation body itself. The amplitude of the electric field $|\vec{E}_0(z)|$ (normalized to the power loss of the cavity \sqrt{P}) can be calculated as

$$\frac{|\vec{E}_0(z)|}{\sqrt{P}} = \sqrt{-4 \frac{Q_0}{\alpha_s} \frac{\Delta\omega(z)}{\omega_0^2}}, \quad (1)$$

where Q_0 is the unloaded quality factor of the DTL prototype, ω_0 is the resonance angular frequency of the DTL prototype without perturbation body, and $\Delta\omega_0$ is the angular frequency shift due to the perturbation at position z . The perturbation body is characterized by the constant α_s . The perturbation body consists of aluminum oxide and is cylindrical ($V = 1 \text{ mm}^3$). The string is made of nylon and has a diameter of 0.25 mm. α_s was determined by measuring the E-field distribution of the reference cavity ($f_R \approx 2998$ MHz) with known R_L (see Table I) using the same bead-pulling setup to $(-5.5 \pm 1.5) \cdot 10^{-21} \frac{\text{Asm}^2}{\text{V}}$. Finally, R_L can be determined by an integration of the normalized E-field to

$$R_L = \left(\int_0^L \frac{|\vec{E}_0(z)|}{\sqrt{P}} dz \right)^2 \frac{1}{L}. \quad (2)$$

The uncertainty on α_s results from the propagation of the uncertainty of the reference cavity's R_L ($\pm 13 \frac{\text{M}\Omega}{\text{m}}$) and of the frequency measurement error of ± 10 kHz using the correlations from Eqs. (1) and (2).

III. RESULTS

A. Basic properties of the DTL prototype

Figure 3 shows the printed DTL prototype assembled with the vacuum flanges, the valves of the cooling system, the excitation loop, the pickup loop, the fixed copper tuner, and the motorized variable copper tuner. A cavity pressure of about $2 \cdot 10^{-7}$ mbar was achieved for the DTL prototype within a few hours using standard equipment to obtain a high vacuum. The cooling system was fundamentally tested whereby no defects were identified. A flow rate of roughly 2 l min^{-1} was measured for a pressure difference of 1 bar between the two valves of the cooling system. For the minimum cross section of the cooling system, this results in a flow velocity of roughly 1 m s^{-1} . Using the tuning rods, the planned resonance frequency of 2998 MHz was achieved at a room temperature of 22°C . Due to the dimensions of the DTL prototype, the geometric accuracy cannot be measured without destroying its cavity. However, the variable tuning rod allows a maximum variation of the resonant

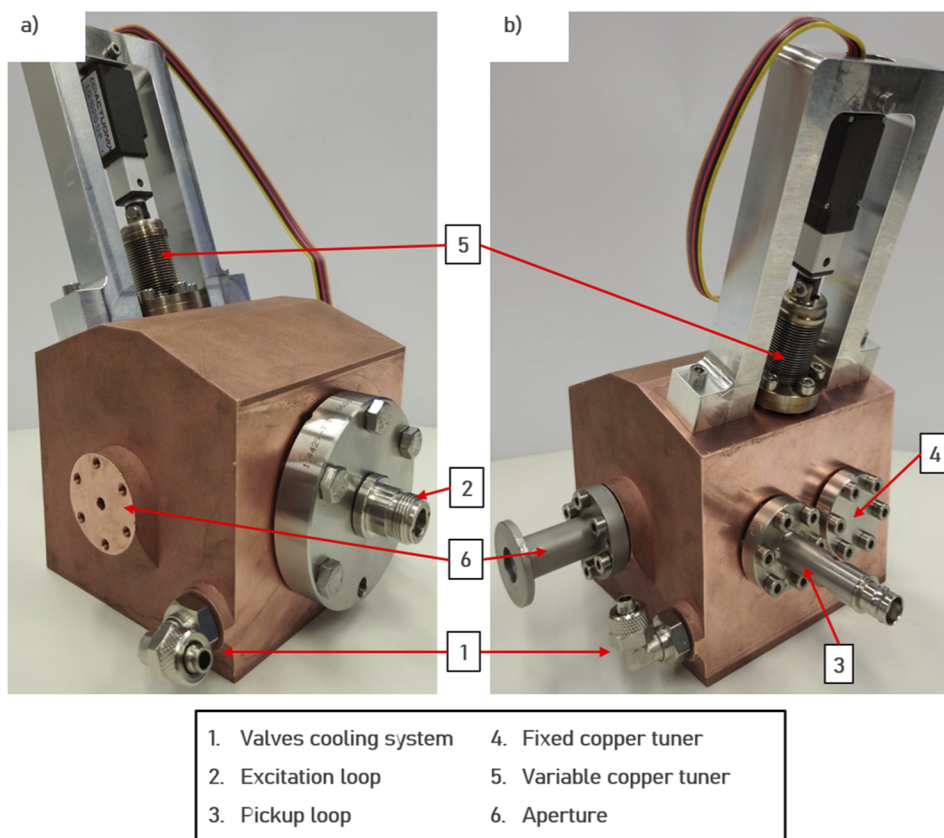


FIG. 3. Front view (a) and rear view (b) of the fully equipped printed DTL prototype.

frequency of around 2 MHz. CST simulations show that changing the cavity diameter by around $60\ \mu\text{m}$ or the length of all gaps by around $20\ \mu\text{m}$ would result in the same variation of the resonance frequency. It can therefore be assumed that the average accuracy of the geometry is less than $60\ \mu\text{m}$. Such values were expected since an accuracy of around $50\ \mu\text{m}$ is typical for the selective laser melting process.³⁵ However, it is imaginable that larger variations of single sub-geometries and the associated shift in resonant frequency are canceled out by “counteracting” geometric variations. Further studies are therefore required to assess the reproducible accuracy with which cavities can be produced using the SLM process. The averaged surface roughness R_a of sub-geometries of the printed DTL prototype (red marked geometries A, B, and C in Fig. 1) is determined as described in Sec. II. R_a was determined at the stem (A), at the cavity top (B), and at the cavity bottom (C) to be 11, 42, and $24\ \mu\text{m}$, respectively.

B. RF performance of the DTL prototype

The measured unloaded quality factor Q_0 of the printed DTL prototype is 8750 ± 484 . The standing wave ratio (SWR) at the excitation loop during the measurement was 1.1. As described in Sec. II C, the shunt impedance per unit length R_L of the printed DTL

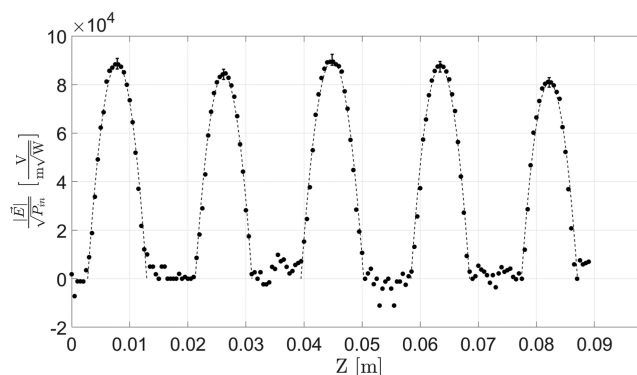


FIG. 4. Electric field distribution along the beam axis ($|\vec{E}(z)|$) as measured for the fundamental TM_{010} -Mode (dots) and corresponding fit for the determination of the shunt impedance per unit length (dashed line).

prototype was determined using the bead-pull method. Figure 4 shows the normalized E-field amplitude along the z axis as measured for the TM_{010} -Mode (dots) and an input power of 7.5 dBm. The corresponding fit for the integration of the normalized

electric field distribution is plotted as a dashed line. The measurement error of the maximum field amplitudes was determined to be $\pm 2.5\%$ by measuring the maximum field amplitudes of the five gaps in five separate measurements over a period of 5 h. Thereby, the thermally induced variation of the resonance frequency (± 15 kHz) contributes $\sim 1.9\%$. Similar to the DTL parts of the SCDTL structure of the TOP-IMPLART project, a thermal drift results in the resonant frequency drift of $\frac{\Delta f}{\Delta T} \approx 46 \frac{\text{kHz}}{^\circ\text{C}}$.³⁶ Using Eq. (1) and assuming that the measurement error of the frequency is ± 10 kHz, the variation of the resonance frequency (± 15 kHz) corresponds to a temperature variation of $\sim \pm 0.3^\circ$. Due to the non-automated measuring process, the measurement of the normalized E-field amplitude along the z axis requires a measuring time of about 3 h. Thereby, similar temperature variations are expected, since the cavity temperature varies with the room temperature due to the not yet existing chiller system. Comparing the normalized E-field distribution over the five gaps, the variation of the maximum amplitude is $\sim \pm 5\%$ to the average. After quadratic substitution of the measurement error resulting from the thermal drift, the variation of the maximum field amplitudes between the gaps is $\sim \pm 4.7\%$ to the average. This variation of the maximal gap amplitudes most likely results from geometrical inaccuracies. Simulations show that this field variation corresponds, for example, to a variation of the gap length of ~ 0.3 mm. However, the variation of the maximum field amplitude is below the variation of $\pm 5\%$ required, e.g., for comparable structures of the TOP-linac and can therefore be accepted.³⁷ The measurements to determine the error of the maximum field amplitudes also allow an evaluation of the spacing between the maximum field amplitudes and thus the unit cell length. These are determined to be 18.3, 18.4, 18.2, and 18.3 mm with an error of about 0.2 mm. The measured cell lengths thus correspond to the design value of 18.2 mm within the measurement uncertainties. Using Eq. (2) and the integration of the normalized electric field distribution, R_L was determined to be $(102 \pm 14) \frac{\text{M}\Omega}{\text{m}}$. The error on R_L is determined via relations (1) and (2). Thereby, the known measurement error of the frequency, the uncertainties on α_s , and the variation of the maximum field amplitude are taken into account.

The presented printed DTL prototype has been operated at a maximum input power P of 1 kW (pulse length: 5 μs and repetition rate: 200 Hz) by using an existing solid-state amplifier over 4 h. Here, thermal changes were compensated by a feedback control loop via the variable tuning rod. In all test measurements, no significant rapid changes of the standing wave ratio (SWR) at the excitation loop or in the quality of the vacuum occurred, which would indicate multipactor effects or breakdown phenomena (electrical discharges, such as vacuum arcs). Using the equation $U = \sqrt{R_L \cdot L \cdot P}$, the input power of 1 kW results in an axial integrated voltage U of $\sim (96 \pm 6)$ kV. This results in a maximum E-field strength of roughly $3.5 \frac{\text{MV}}{\text{m}}$ for the specified gap length of 5.55 mm. Considering the corresponding transit time factor of ~ 0.71 for 16 MeV protons, a buncher amplitude of $\sim (68 \pm 5)$ kV results for the planned pre-clinical proton minibeam irradiation facility. As part of the TOP-IMPLART^{22,23} or LIGHT project,²⁴ similar linac structures are powered by klystron amplifiers via waveguides with a few hundred kW (5 μs @ 200 Hz). Whether the surface quality of the shown DTL prototype limits high gradient operation as in the TOP-IMPLART or LIGHT project ($>40 \frac{\text{MV}}{\text{m}}$) remains to be evaluated by similar studies as described in Ref. 38.

IV. DISCUSSION

A. Comparison with a traditionally manufactured structure

The performance of the 3D printed DTL prototype is compared with the traditionally manufactured DTL structure adapted from the TOP-IMPLART SCDTL-2 module. Each drift tube of the reference structure is supported by two stems. Both stems are comparable in volume and position to the one stem of the printed DTL prototype. The measured Q_0 and R_L as well as the dimensions of the reference structure are also shown in Table I.

The accuracy of the SLM printing process is sufficient to produce a DTL cavity of the type shown, achieving a specific resonance frequency without post-processing. However, it should be mentioned that the geometric accuracy of the 3D printed cavity is reduced by a factor of 6 compared to the traditionally manufactured cavity. This reduction may no longer be compensated by a tuning rod for cavities with a resonant frequency significantly higher than 3 GHz.

The measured Q_0 of the DTL prototype is reduced by about 33% compared to the CST simulation (and thus to the expected values) and about 15% compared to the traditionally manufactured reference cavity (see Table I). For R_L , a reduction of 26% was measured compared to the simulation (and thus to the expected values) and 4% compared to the traditionally manufactured reference cavity (see Table I). The calculated axial voltage achieved with an input power of 1 kW is by far sufficient to use the printed DTL prototype as a buncher unit for the planned pre-clinical irradiation facility. The results show that 3D printing is already an alternative to traditional techniques for the manufacturing of DTL structures that are not operated at high E-field strengths ($>3.5 \frac{\text{MV}}{\text{m}}$). Due to the manufacturing costs reduced by a factor of 3 (compared to the reference cavity), the slightly reduced performance of the printed cavity can be potentially compensated in many cases by using more powerful RF sources or additional/larger linac structures. Naturally, it must be taken into account here that a 26% stronger RF source or more/larger structures to compensate for the 26% reduction in shunt impedance (compared to the simulation) will also incur costs. It should be emphasized that these promising results were achieved because the 3D printing process allows the production of DTL structures with only one stem per drift tube without great effort. The performance differences (Q_0 and R_L) between the simulation and measurement for the 3D printed structure most likely result from the rather high surface roughness ($R_a > 11 \mu\text{m}$) and associated Ohmic RF power losses in the 3D printed cavity walls. Compared to the traditionally manufactured cavity, where there is no difference (within the uncertainties) between simulated and measured Q_0 and R_L , respectively, R_a of the 3D printed cavity is increased by more than a factor of 10. Especially when operating at high frequencies, enhanced surface roughness increases RF power losses and favors breakdown phenomena.³⁹ Further improvement of the structure is therefore focused on reducing surface roughness through optimized parameters for additive manufacturing of copper and post-processing of the inner cavity surface. Examples of such post-machining approaches include mass finishing, chemical etching, chemical-mechanical polishing, electropolishing, or magnetically driven abrasive polishing.^{39–41}

B. Potential of 3D printing for RF cavities

The fundamental potential of 3D printing for the production of cavity geometries was demonstrated using a DTL geometry. In addition to the reasons explained in Sec. II A, the DTL geometry was also chosen because DTL cavities are among the most frequently used structures for accelerator systems. This illustrates that the potential of 3D printing processes is not limited to special application cases. Although more research is needed to match (or exceed) the RF performance of traditionally manufactured structures, the realized single-stem geometry with integrated cooling channels already demonstrates the significantly greater design freedom of the 3D printing process. A variety of cavity geometries are used worldwide for a wide range of tasks, whereby the RF performance is not necessarily the only limiting factor. Due to the complexity of the subject, an overview of the potential improvements that can be achieved through the use of 3D printing processes for various cavity applications cannot be given in this study. Nevertheless, some examples of design possibilities that are not or only with difficulty realizable with conventional manufacturing processes and applications for cavities are given in the following. The gain in geometric design freedom enables, among other things: (1) The realization of completely new cavity geometries. (2) The possibility to manufacture already known concepts (e.g., spiral resonators) in smaller dimensions and at the same time much more filigree than currently possible. (3) Finer meshed cooling systems, which can be integrated closer to the surface of the cavity's inner walls, allowing for more efficient and stable operation. In addition to the geometric design freedom, another advantage of 3D printing is the ability to manufacture parts from a combination of different materials (in the case of SLM metals) without much effort. Thus, the so-called multi-material printing allows us to use thermal, electromagnetic, or other material properties targeted and locally, which leads to the following considerations: (1) Certain sections of the geometry could be thermally decoupled by incorporating an area of thermally poorly conducting material, such as stainless steel (possibly as a non-dense honeycomb print). The temperature of areas with high current density could thus be greatly reduced to lower the thermal resistance, while the outer cavity body would remain at room temperature. (2) In addition, only the geometry parts that are thermally or electrically relevant, such as the inner cavity surfaces, could be printed from, e.g., copper and the rest of the cavity body from, e.g., stainless steel. Thus, for example, it would be possible for high-frequency cavities to achieve high RF performance due to the skin effect, while at the same time improving the mechanical properties of the cavity body.

The examples given above are only to be seen as suggestions for future research and must therefore first be evaluated for feasibility. Nevertheless, in addition to the DTL prototype presented, they clearly illustrate the potential of 3D printing technology for the manufacturing of cavity structures.

V. CONCLUSION

Selective laser melting, although in some detail inferior to electron beam melting, has recently started to provide good access for the research community through its commercial distribution. For the first time, a drift tube linac prototype has been manufactured with the cavity entirely 3D printed from high-purity copper using

selective laser melting. Compared to a similar structure produced with traditional manufacturing methods and to CST simulations, the resulting performance is only slightly reduced. At the same time, production costs are reduced by a factor of 3 through the use of 3D printing. It is expected that the production costs of 3D printing may be reduced by a similar factor also for producing such structures in series. Material consumption and printing costs can be further reduced by recalculating the material thicknesses of the walls under the condition of stable mechanical and electromagnetic performance. The cavity geometry modifications to avoid post-processing steps (such as removal of support structures) can also be applied to other RF cavity types (side coupled drift tube linac, coupled-cavity linac, etc.) and dimensions. Although the DTL prototype still needs to be tested at E-field strengths $>3.5 \frac{\text{MV}}{\text{m}}$, the results show that 3D printing is already an alternative to conventional manufacturing methods for cavity structures in many cases. For the first time, it is now possible to print a wide variety of prototypes and maybe even entire accelerators from high-purity copper. Together with the high freedom in structural design, the possibilities of multi-material printing, and the potential to drastically reduce the cost of manufacturing, it may revolutionize the field of manufacturing RF cavities.

ACKNOWLEDGMENTS

We acknowledge financial Support by EU Project Radiate.

AUTHOR DECLARATIONS

Conflict of Interest

The authors have no conflicts to disclose.

DATA AVAILABILITY

The data that support the findings of this study are available from the corresponding author upon reasonable request.

REFERENCES

- ¹S. Witman, "Ten things you might not know about particle accelerators," in *Symmetry Magazine* (Fermi National Accelerator Laboratory, 2014), Vol. 21.
- ²M. G. Pullia, "Synchrotrons for hadrontherapy," *Rev. Accel. Sci. Technol.* **2**, 157–178 (2009).
- ³D. L. Friesel and T. A. Antaya, "Medical cyclotrons," *Rev. Accel. Sci. Technol.* **2**, 133–156 (2009).
- ⁴U. Amaldi, S. Braccini, and P. Puggioni, "High frequency linacs for hadrontherapy," *Rev. Accel. Sci. Technol.* **2**, 111–131 (2009).
- ⁵U. Amaldi, R. Bonomi, S. Braccini, M. Crescenti, A. Degiovanni, M. Garlasché, A. Garonna, G. Magrin, C. Mellace, P. Pearce *et al.*, "Accelerators for hadrontherapy: From Lawrence cyclotrons to linacs," *Nucl. Instrum. Methods Phys. Res., Sect. A* **620**, 563–577 (2010).
- ⁶I. H. Wilson, "Cavity construction techniques," in Proceedings of the CERN Accelerator School of RF Engineering for Particle Accelerators, Oxford, 1991.
- ⁷S. Ghodke, R. Barnwal, J. Mondal, A. Dhavle, S. Parashar, M. Kumar, S. Nayak, D. Jayaprakash, V. Sharma, S. Acharya *et al.*, "Machining and brazing of accelerating RF cavity," in *2014 International Symposium on Discharges and Electrical Insulation in Vacuum (ISDEIV)* (IEEE, 2014), pp. 101–104.
- ⁸L. Picardi, C. Ronsivalle, and B. Spataro, "Design development of the SCDTL structure for the TOP linac," *Nucl. Instrum. Methods Phys. Res., Sect. A* **425**, 8–22 (1999).

- ⁹J.-M. Lagniel and F. DSM-DAPNIA-SEA, "Linac architecture for high power proton sources," in XX International Linac Conference, Monterey, 2000.
- ¹⁰F. Calignano, D. Manfredi, E. P. Ambrosio, S. Biamino, M. Lombardi, E. Atzeni, A. Salmi, P. Minetola, L. Iuliano, and P. Fino, "Overview on additive manufacturing technologies," *Proc. IEEE* **105**, 593–612 (2017).
- ¹¹A. Grudiev, "Additive manufacturing for RF applications," CERN, BE-RF, 2014; available at https://indico.cern.ch/event/333735/contributions/779090/attachments/651308/895576/Grudiev_-_Additive_Manufacturing_4RF_AG.pdf.
- ¹²M. D'Auria, W. J. Otter, J. Hazell, B. T. Gillatt, C. Long-Collins, N. M. Ridler, and S. Lucyszyn, "3-D printed metal-pipe rectangular waveguides," *IEEE Trans. Compon., Packag., Manuf. Technol.* **5**, 1339–1349 (2015).
- ¹³B. Zhang and H. Zirath, "Metallic 3-D printed rectangular waveguides for millimeter-wave applications," *IEEE Trans. Compon., Packag., Manuf. Technol.* **6**, 796–804 (2016).
- ¹⁴P. Frigola, R. Agustsson, G. Ciovati, W. Clemens, P. Dhakal, L. Faillace, F. Marhauser, J. Mireles, P. Morton, A. Murokh *et al.*, "Advance additive manufacturing method for SRF cavities of various geometries," in *Proceedings of the SRF 2015* (JACoW, 2015), pp. 1181–1184.
- ¹⁵D. L. Creedon, M. Goryachev, N. Kostylev, T. B. Sercombe, and M. E. Tobar, "A 3D printed superconducting aluminium microwave cavity," *Appl. Phys. Lett.* **109**, 032601 (2016).
- ¹⁶R. Gerard, "Additive manufacturing for RF and superconducting RF applications," in Proceedings of the Colloque Fabrication Additive Physique des Deux Infinis (Bures-sur-Yvette, France, 2018), Vol. 14.
- ¹⁷T. Q. Tran, A. Chinnappan, J. K. Y. Lee, N. H. Loc, L. T. Tran, G. Wang, V. V. Kumar, W. A. D. M. Jayathilaka, D. Ji, M. Doddamani, and S. Ramakrishna, "3D printing of highly pure copper," *Metals* **9**, 756 (2019).
- ¹⁸P. Frigola, O. Harrysson, T. Horn, H. West, R. Aman, J. Rigsbee, D. Ramirez, F. Medina, R. Wicker, and E. Rodriguez, "Fabricating copper components with electron beam melting," *Adv. Mater. Processes* **172**(7), 20–24 (2014).
- ¹⁹J. Huber, "Could the next generation of particle accelerators come out of the 3D printer?," (SLAC National Accelerator Laboratory, 2020); available at <https://www6.slac.stanford.edu/news/2020-02-05-could-next-generation-particle-accelerators-come-out-3d-printer.aspx>.
- ²⁰T.-T. Ikeshoji, K. Nakamura, M. Yonehara, K. Imai, and H. Kyogoku, "Selective laser melting of pure copper," *JOM* **70**, 396–400 (2018).
- ²¹PROTIQ GmbH, Blomberg, Germany, 2020.
- ²²P. Nenzi, A. Ampollini, G. Bazzano, F. Marracino, L. Picardi, C. Ronsivalle, V. Surrenti, M. Vadrucchi, C. Snels, E. Casaccia *et al.*, "Status of the TOP-IMPLART proton LINAC," in TUPWI004, These Proceedings, IPAC015, Richmond, VA, 2015.
- ²³C. Cianfarani, E. Cisbani, G. Orlandi, S. Frullani, L. Picardi, and C. Concetta Ronsivalle, "Status of the TOP Linac project," *Nucl. Instrum. Methods Phys. Res., Sect. A* **562**, 1029–1032 (2006).
- ²⁴A. Degiovanni, P. Stabile, D. Ungaro, and A.D.A.M. SA, "Light: A linear accelerator for proton therapy," in Proceedings of NAPAC2016, Chicago, 2016.
- ²⁵Dassault Systèmes, CST Studio suite, 2016.
- ²⁶M. Mayerhofer, G. Datzmann, A. Degiovanni, V. Dimov, and G. Dollinger, "Magnetically focused 70 MeV proton minibeam for preclinical experiments combining a tandem accelerator and a 3 GHz linear post accelerator," *Med. Phys.* **48**, 2733 (2020).
- ²⁷Siemens PLM Software, Solid edge, 2017.
- ²⁸M. Mayerhofer, A. Bergmaier, G. Datzmann, H. Hagn, R. Helm, J. Mitteneder, R. Schubert, L. Picardi, P. Nenzi, C. Ronsivalle *et al.*, "Concept and performance evaluation of two 3 GHz buncher units optimizing the dose rate of a novel preclinical proton minibeam irradiation facility," *PLoS One* **16**, e0258477 (2021).
- ²⁹M. Mayerhofer and G. Dollinger, "Manufacturing method for radio-frequency cavity resonators and corresponding resonator" European patent application No. 20 187438.5.
- ³⁰T. P. Wangler, *RF Linear Accelerators* (John Wiley & Sons, 2008), pp. 42–44.
- ³¹L. C. Maier, Jr. and J. C. Slater, "Field strength measurements in resonant cavities," *J. Appl. Phys.* **23**, 68–77 (1952).
- ³²P. A. McIntosh, "Perturbation measurements on RF cavities at Daresbury," in 4th European Particle Accelerator Conference (Daresbury Laboratory, London, 1994), p. 1283, <https://cds.cern.ch/record/922175>.
- ³³R. A. Waldron, "Perturbation theory of resonant cavities," *Proc. IEE Part C: Monogr.* **107**, 272–274 (1960).
- ³⁴J. C. Slater, *Microwave Electronics* (van Nostrand, New York, 1950), Vol. 80.
- ³⁵W. S. W. Harun, N. S. Manam, M. S. I. N. Kamariah, S. Sharif, A. H. Zulkify, I. Ahmad, and H. Miura, "A review of powdered additive manufacturing techniques for Ti-6al-4v biomedical applications," *Powder Technol.* **331**, 74–97 (2018).
- ³⁶M. Ciambrella, F. Cardelli, M. Migliorati, A. Mostacci, L. Palumbo, L. Ficcardenti, V. Pettinacci, L. Picardi, and C. Ronsivalle, "Electromechanical analysis of SCDTL structures," in *5th International Particle Accelerator Conference (IPAC'14)*, Geneva, Switzerland, 15–20 June 2014, <http://www.jacow.org>, pp. 3250–3252.
- ³⁷L. Picardi, C. Ronsivalle, and A. Vignati, "Measurement of cavities of the side coupled drift tube linac (SCDTL)," in Proceedings of EPAC96, TH002A, 1996.
- ³⁸A. Degiovanni, R. Bonomi, M. Garlasché, S. Verdú-Andrés, R. Wegner, and U. Amaldi, "High gradient RF test results of S-band and C-band cavities for medical linear accelerators," *Nucl. Instrum. Methods Phys. Res., Sect. A* **890**, 1–7 (2018).
- ³⁹A. H. Seltzman and S. J. Wukitch, "Surface roughness and finishing techniques in selective laser melted GRCo-84 copper for an additive manufactured lower hybrid current drive launcher," *Fusion Eng. Des.* **160**, 111801 (2020).
- ⁴⁰I. Karakurt, K. Y. Ho, C. Ledford, D. Gamzina, T. Horn, N. C. Luhmann, and L. Lin, "Development of a magnetically driven abrasive polishing process for additively manufactured copper structures," *Procedia Manuf.* **26**, 798–805 (2018).
- ⁴¹A. Zarrebini-Esfahani, M. Aslaninejad, M. Ristic, and K. Long, "Experimental analysis of surface finish in normal conducting cavities," *Nucl. Instrum. Methods Phys. Res., Sect. A* **869**, 76–83 (2017).